Electron. Mater. Lett., Vol. 11, No. 3 (2015), pp. 409-415
DOI: 10.1007/s13391-014-3293-5

Photoluminescent Properties of Tb^{3+} Doped $GdSrAl_3O_7$ Nanophosphor Using Solution Combustions Synthesis

Satyender Pal Khatkar, Sonika Singh, Sheetal Lohra, Avni Khatkar, and Vinod Taxak*

Department of Chemistry, Maharshi Dayanand University, Rohtak-124001, India

(received date: 14 October 2014 / accepted date: 15 October 2014 / published date: 10 May 2015)

A color tunable terbium doped $GdSrAl_3O_7$ nanophosphor has been synthesized at low temperature using solution combustion synthesis. The photoluminescent properties of nanophosphors have been explored by analyzing their excitation and emission spectra alongwith their decay curves. The emission spectra exhibit dominating green light at 544 nm due to $^5D_4 \rightarrow {}^7F_5$ transition of Tb^{3+} ions in $GdSrAl_3O_7$ on excitation by UV light of 239 nm. Furthermore, the luminescence in $Gd_{(1-x)}SrAl_3O_7$: xTb^{3+} nanophosphors shifted from blue to green color by properly tuning the concentration of terbium ions. Decay curves indicate that non-radiative cross-relaxation is primarily responsible for concentration quenching phenomenon in the $GdSrAl_3O_7$ host. X-ray diffraction (XRD) analysis confirmed that single tetragonal phased nanophosphor could be readily obtained at low temperature 550°C. The smooth surfaced nanocrystals with particle size of 45 - 50 nm have also been examined by transmission electron microscopy (TEM). All these features augmented the probability of $GdSrAl_3O_7$: Tb^{3+} nanophosphor for potential applications in optical devices.

Keywords: solution combustion synthesis, photoluminescent, $GdSrAl_3O_7$, nanophosphor

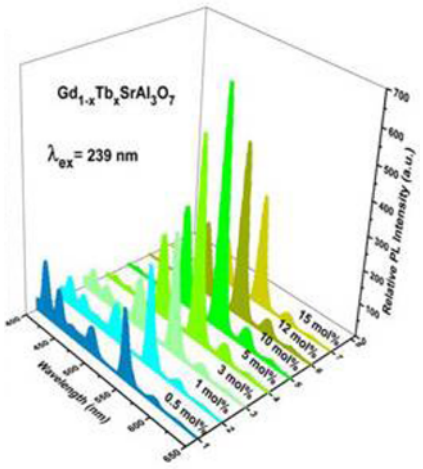

1. INTRODUCTION

In the past few years much progress has been made to develop rare-earth doped nanomaterials for their possible applications in the fields of luminescent devices, biochemical probes, optical transmission, and medical diagnostics.[1-5] Rare earth (RE^{3+}) phosphors possess great chemical stability, high luminescence efficiency and flexible emission colors with different dopants.[6,7] More attention has been paid to unique spectroscopic characteristics of lanthanides resulted from 4f shell of the ions. The 4f emission spectra of RE^{3+} exhibits narrow lines with high color purity as 4f electrons are well shielded by outer 5s and 5p electrons.[8-10] As a kind of melitite structure, lanthanide pervoskite ABC_3O_7 (A=Ca, Sr, Ba; B=Y, La, Gd and C=Al, Ga) doped with RE^{3+} ions show efficient luminescence in the visible range which make them essential to advanced display perspectives.[11-20] These compounds crystallize in tetragonal sheet-like arrangement belonging to the space group *P*- 42_1m. The crystal structure consists of CO_4^{5-} tetrahedral layers in the *ab* plane, perpendicular to *c*-axis. A^{2+} ions and B^{3+} ions are randomly distributed inbetween the layers occupying the eight coordinated sites with Cs symmetry while C^{3+} cations occupy two non-equivalent tetragonal sites with site symmetries S_4 and Cs respectively.[21-26]

In the rare-earth family, trivalent terbium ion is a significant dopant with strong emission around 544 nm which is found to be very close to the theoretical optimum wavelength for the green component of three primary color centers.[27] Tb^{3+} doped phosphors have been proved excellent green luminescent materials to replace commercially available Mn^{2+} doped phosphors due to better thermal stability, high brightness, less out gassing, chemical inertness and shorter decay time.[28] Thus, there is a renewed vigor among the researchers for new efficient green phosphors with short decay time. Tb^{3+} doped $GdSrAl_3O_7$ green phosphor has been investigated by Zhou et. al using EDTA sol-gel process, which reports the existence of phase-pure $GdSrAl_3O_7$ only at high sintering temperature (900°C for 5 h).[18] In this context, solution combustion synthesis (SCS) turns to be best way to synthesize this phosphor with good homogeneity,

*Corresponding author: v_taxak@yahoo.com

crystallinity and high surface area in a very short duration of time at low temperature. In SCS, it is easy to control stoichiometry due to well mixing of reaction components at the molecular level in homogenous liquid precursor. In addition, this short synthesis process generates intense heat, sufficient to produce fine well-crystallized phosphors.[29,30]

Herein, to the best of our knowledge this is the first report on synthesis of terbium doped $GdSrAl_3O_7$ nanophosphor at low temperature using solution combustion approach. It has been noticed that Gd^{3+} ions in the host lattice acts as sensitizer for the luminescence, resulting in improved efficiency of phosphor due to efficient energy transfer from host to activator via intermediate energy levels. In this host, Tb^{3+} ions exhibits blue emission due to $^5D_3 \rightarrow {}^7F_{5\text{-}3}$ transitions at low concentration and green emission corresponding to transitions from excited $^5D_4$ level to the $^7F_{6\text{-}3}$ states at high concentration, out of which $^5D_4 \rightarrow {}^7F_5$ transition at 544 nm being strongest. Luminescence in $Gd_{(1-x)}SrAl_3O_7$: xTb^{3+} nanophosphors could be tuned from blue to green on varying the concentration of terbium ions. Decay curves and energy transfer mechanism of concentration quenching phenomenon in Tb^{3+} doped $GdSrAl_3O_7$ nanophosphors were also investigated. The strong emission and controllable light color make it suitable for application in advanced lighting and display fields.

2. EXPERIMENTAL PROCEDURE

2.1 Powder synthesis

Powder samples of $Gd_{1-x}SrAl_3O_7$: xTb^{3+} nanophosphors were synthesized using urea assisted solution combustion process. The chemical equation for the reaction was:

$$1\text{-}xGd(NO_3)_3 + xTb(NO_3)_3 + Sr(NO_3)_2 + 3Al(NO_3)_3 + 11.66CH_4N_2O \rightarrow Gd_{1-x}Tb_xSrAl_3O_7(s) + \text{gaseous products.} \quad (1)$$

High purity raw materials $Sr(NO_3)_2$, $Gd(NO_3)_3.6H_2O$, $Al(NO_3)_3.9H_2O$, $Tb(NO_3)_3.6H_2O$ and urea were taken according to nominal composition of $Gd_{1-x}SrAl_3O_7$: xTb^{3+}, where x = 0.005 to 0.15 and dissolved in minimum quantity (40 mL) of deionized water in 200 mL capacity Pyrex beaker. The solution was stirred thoroughly to ensure molecular level mixing of precursors, resulting in a clear and homogenous solution. The amount of urea was calculated using total oxidizing and reducing valencies according to the concept used in propellant chemistry.[31] Finally the beaker containing the solution was placed in a preheated furnace maintained at 500°C. The materials undergo rapid dehydration and foaming followed by decomposition, generating combustible gases. The volatile combustible gases ignite and burn with a flame yielding voluminous solid within 5 - 8 min. The sample thus obtained was again fired at 550°C for 1 h in order to obtain single phased $Gd_{1-x}Tb_xSrAl_3O_7$ nanophosphor. SCS being a self sustained highly exothermic redox reaction in homogenous solution of oxidizer (metal nitrates) and fuel (urea), releases intense chemical energy to heat the system to high temperatures (>1000°C) in few minutes.[32] This leads to the high product purity of Tb^{3+} doped $GdSrAl_3O_7$ nanophosphors at low crystalline temperature via SCS in comparision to EDTA sol-gel process[18] as volatile impurities are extracted to be expelled out due to attainment of high temperature in self- propagating solution combustion process.

2.2 Powder characterization techniques

The structural characteristics of $Gd_{1-x}Tb_xSrAl_3O_7$ powders were identified by x-ray diffraction (XRD) patterns in the 2θ range of 15 - 70° using Rigaku Ultima-IV x-ray powder diffractometer with Cu$K\alpha$ radiation at 40 kV tube voltage and 40 mA tube current. The Fourier transform infra-red (FT-IR) was recorded on Perkin-Elmer spectrometer in the spectral range 4000 - 400cm^{-1}. The morphology and particle size were obtained using Hitachi F-7500 transmission electron microscope (TEM). The photoluminescence excitation and emission spectra of the nanophosphor in the ultraviolet-visible region and decay curves under time scan-mode were measured on Hitachi F-7000 fluorescence spectrophotometer equipped with Xe-lamp as an excitation source. The life time of the nanophosphor was calculated by the software of the spectrophotometer (FL solution for F-7000).

3. RESULTS AND DISCUSSION

$GdSrAl_3O_7$ have layered tetragonal structure of melitite type ABC_3O_7 belonging to space group P-42$_1$m with the lattice parameter $a = b = 7.801$ A° and $c = 5.132$ A°. In strontium gadolinium aluminate pervoskite $GdSrAl_3O_7$, the frames of the lattice are formed by five-membered rings constructed from tetrahedral AlO_4^{5-} linked at each corner. The Sr^{2+} ions and Gd^{3+} ions are randomly distributed at the centers of these rings with Cs symmetry. Figure 1a depicts the XRD profiles of $Gd_{0.90}Tb_{0.10}SrAl_3O_7$ nanoparticles as synthesized and sintered at 550°C. All the XRD peaks coincide well with standard diffraction data of $GdSrAl_3O_7$ (JCPDS No. 50-1817), confirming that tetragonal phase of $GdSrAl_3O_7$ powders can be readily obtained at 500°C furnace temperature within few minutes using SCS. Although some minor peaks ascribed as '*' due to those of undecomposed nitrates were also detected in the XRD pattern. These background peaks disappeared completely on sintering the sample at 550°C for 1 h, with no significant change in intensity of main peak. The reason for lower crystallization temperature by SCS may be attributed to two aspects; molecular level mixing of constituent metal ions and attainment of high temperature in a short period of time due to ignition of an organic fuel and nitrates at low furnace

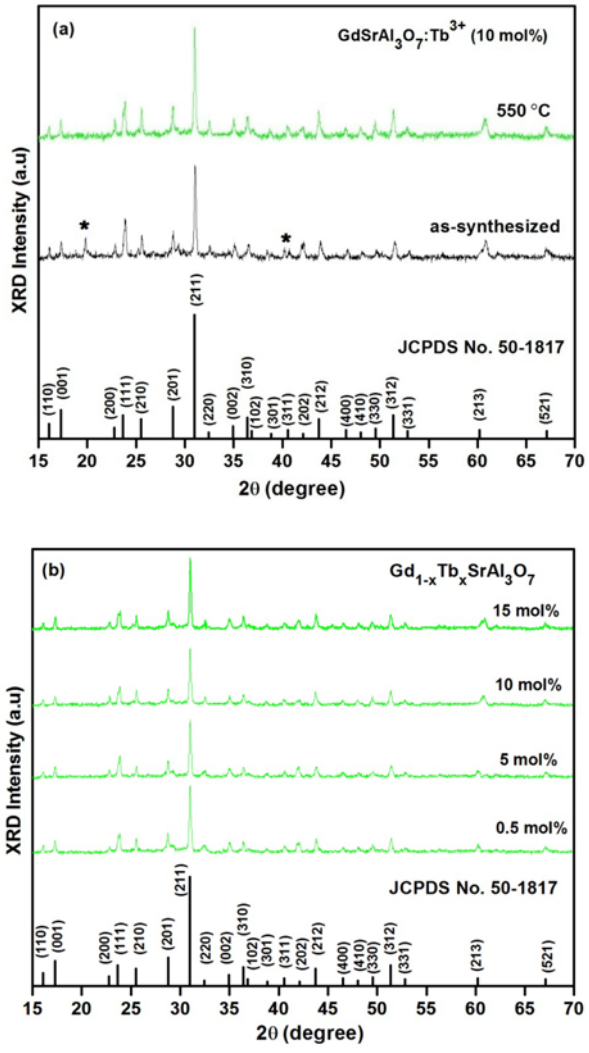

Fig. 1. XRD patterns of (a) $Gd_{0.90}Tb_{0.10}SrAl_3O_7$ powder as synthesized and sintered at 550°C, (b) $Gd_{1-x}Tb_xSrAl_3O_7$ nanophosphor (Tb^{3+} = 0.5, 5, 10 and 15 mol. %) sintered at 550°C alongwith standard data of $GdSrAl_3O_7$ (JCDPS No. 50-1817).

temperature (500°C) during pre-sintering process.

Figure 1(b) illustrates the XRD profiles of $GdSrAl_3O_7$ nanophosphors doped with different terbium contents and sintered at 550°C. No secondary phase corresponding to the doped component was detected, indicating that Tb^{3+} ions completely replaced the Gd^{3+} ions in the $GdSrAl_3O_7$ host lattice due to similar ionic radii of Tb^{3+} (R_{Tb3+} = 0.98 A°) and Gd^{3+} (R_{Gd3+} = 1.00 A°). The average particle size of $Gd_{1-x}Tb_xSrAl_3O_7$ powders was calculated from full width at half maxima (FWHM) of the most intense peak (211) using the well known Debye Scherrer's equation,

$$D = 0.941\lambda/\beta\cos\theta \quad (2)$$

where D is the average grain size, λ the x-ray wavelength (0.1548 nm), and θ and β are the diffraction angle and full width at half-maximum (FWHM, in radian) of an observed peak, respectively. Table 1 gives the values of diffraction angle (2θ) and FWHM for the most intense peak (211) with corresponding particles sizes for different $Gd_{1-x}Tb_xSrAl_3O_7$ powders. It is observed that there is slight variation in the peak position and particles size with different concentrations of Tb^{3+} ions. However, the shift is very small due to the weak change in terbium concentration.

Table 1. Value of 2θ, FWHM and particle size corresponding to the most intense (211) peak for $Gd_{1-x}Tb_xSrAl_3O_7$ nanophosphors sintered at 550°C.

$Gd_{1-x}Tb_xSrAl_3O_7$	2θ (degree)	FWHM (degree)	Particle size (nm)
0.5 mol. %	30.9652	0.1725	49.9
5 mol. %	30.9793	0.172	50.0
10 mol. %	30.987	0.1614	53.3
15 mol. %	31.005	0.1535	56.1

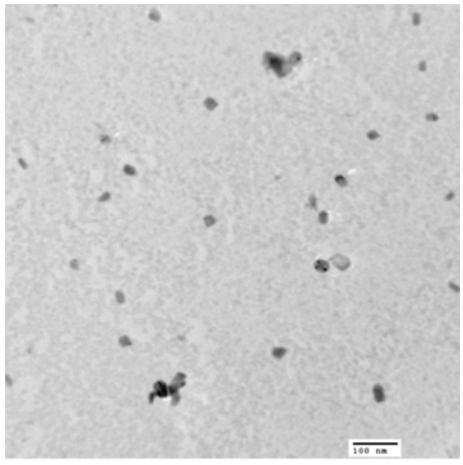

Fig. 2. TEM micrograph of $Gd_{0.90}Tb_{0.10}SrAl_3O_7$ nanophosphor sintered at 550°C.

The surface morphology and particle size of terbium doped $GdSrAl_3O_7$ nanophosphor have been evaluated by transmission electron microscopy. Figure 2 displays the TEM micrograph of 10 mol. % Tb^{3+} doped $GdSrAl_3O_7$ nanophosphor sintered at 550°C. It reveals randomly distributed nearly tetragonal particles having average particle size in the range of 45 - 50 nm. The particle size estimation from TEM studies was in good agreement with that calculated by Scherrer's equation. In comparision to EDTA sol-gel synthesized Tb^{3+} doped $GdSrAl_3O_7$ phosphor, the size distribution of regularly shaped particles obtained by solution combustion synthesis is narrower. The sol-gel synthesized powders as reported by Zhou *et al.*[18] comprised particles having sizes 150 - 300 nm range while pure, more homogeneous and non-agglomerated particles in the nano-regime are obtained by low temperature SCS. This kind of morphology is highly beneficial for the production of

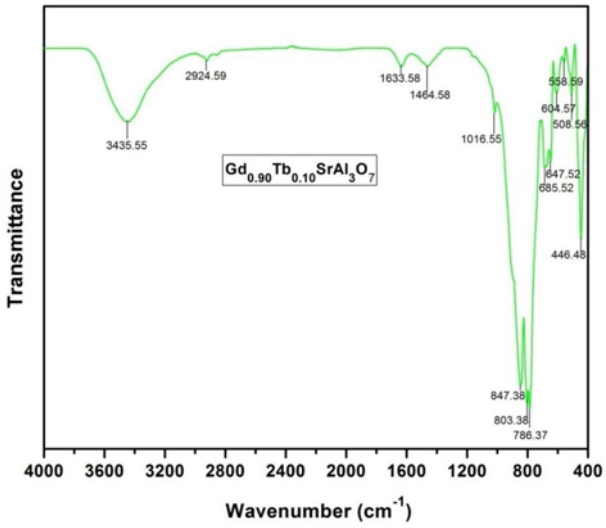

Fig. 3. FT-IR spectrum of $Gd_{0.90}Tb_{0.10}SrAl_3O_7$ nanophosphor sintered at 550°C.

efficient phosphors having advanced optical applications.

Figure 3 depicts the Fourier transform infra-red (FT-IR) spectrum of $Gd_{0.90}Tb_{0.10}SrAl_3O_7$ powder sintered at 550°C. No peak at 1384 cm^{-1} attributed to residual NO_3^- in the sample appear in the spectrum showing pure phase formation at crystallization temperature 550°C, which is several hundred degrees lower than that of EDTA sol-gel method. Strong peaks in the 400 - 900 cm^{-1} region are due to several M-O stretching and bending vibrations of AlO_4^{5-} group in the melitite structure. Besides this, the fundamental H_2O vibration modes at 3435 cm^{-1} due to O-H stretching vibration and minor peak at 1635 cm^{-1} due to H-O-H bending vibrations of water or moisture from air physically absorbed on the sample surface were also observed. The FT-IR results obtained well matched with the XRD studies.

Figures 4(a) and 4(b) illustrate the photoluminescence excitation (PLE) and emission (PL) spectra of $Gd_{0.90}Tb_{0.10}SrAl_3O_7$ nanocrystals sintered at 550°C, respectively. The PLE spectrum of $Gd_{0.90}Tb_{0.10}SrAl_3O_7$ sintered at 550°C, obtained by monitoring the green 544 ($^5D_4 \rightarrow {}^7F_5$) emission, revealed a dominant band ranging from 200 to 250 nm and several excitation peaks in 250 - 400 nm wavelength region. The broad excitation band (200 - 250) with maxima at 239 nm is ascribed to spin allowed transitions (f-d) from the $^7F_6$ ground state of Tb^{3+} ions ($4f^8$) to the excited states of the $4f^75d^1$ electronic configuration.[33] Two narrow bands centered at 272 nm and 313 nm represents the transitions of Gd^{3+} ions from ground state ^8S to excited states ^6I and ^6P, respectively in the $Gd_{1.90}Tb_{0.10}SrAl_3O_7$ nanophosphor. The existence of the absorption due to Gd^{3+} ions indicates energy transfer from Gd^{3+} to Tb^{3+} ions, showing Gd^{3+} acts as sensitizer ions in the host lattice.[20] The other several excitation bands in the wavelength region from 325 to 400 nm correspond to

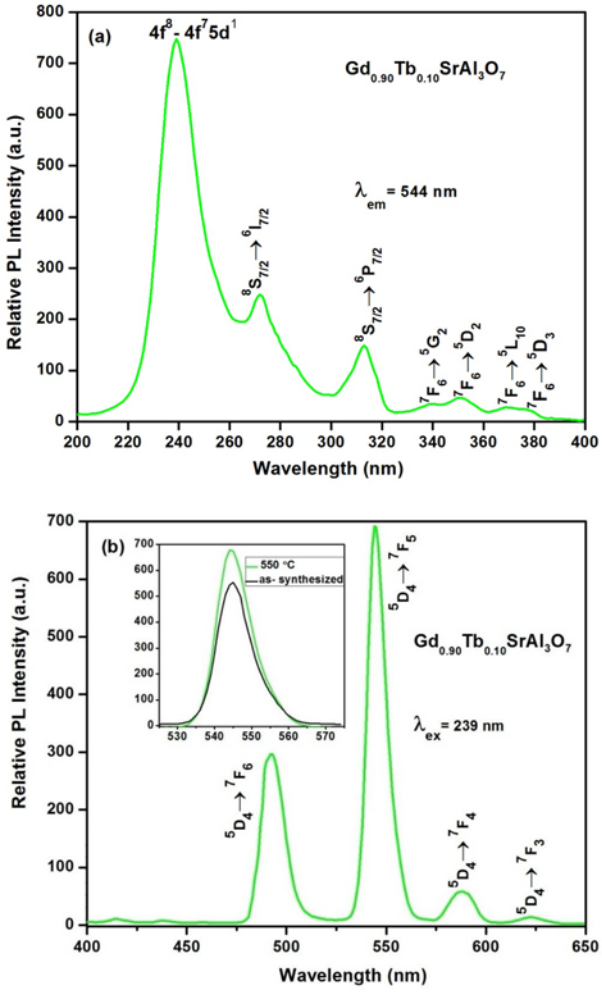

Fig. 4. (a) Photoluminescence excitation of $Gd_{0.90}Tb_{0.10}SrAl_3O_7$ nanophosphor sintered at 550°C, λ_{em} = 544 nm and (b) emission spectra of $Gd_{0.90}Tb_{0.10}SrAl_3O_7$ nanophosphor sintered at 550°C, λ_{ex} = 239 nm (the inset shows the dependence of intensity of 544 ($^5D_4 \rightarrow {}^7F_5$) emission on temperature.

the intrashell f-f transitions of Tb^{3+} ions. These bands could be assigned to the relevant transitions from ground state ($^7F_6$) to the higher energy levels such as $^5G_2$ (339 nm), $^5D_2$ (351 nm), $^5L_{10}$ (369 nm) and $^5D_3$ (379 nm).[34,35] The PL spectrum of $Gd_{0.90}Tb_{0.10}SrAl_3O_7$ nanophosphor sintered at 550°C on monitoring the excitation at 239 nm, exhibits characteristics green emission of Tb^{3+} ions at 492 nm, 544 nm, 588 nm and 622 nm, corresponding to $^5D_4 \rightarrow {}^7F_J$ (J = 6,5,4,3) transitions. The inset of Fig. 4b shows the influence of rise in temperature on the emission intensity of dominant peak at 544 nm assigned to $^5D_4 \rightarrow {}^7F_5$ transition. It was observed that on sintering $Gd_{0.90}Tb_{0.10}SrAl_3O_7$ nanophosphor at 550°C, the emission intensity increased as optimum crystallinity was achieved due to decreased defects in crystals while further sintering of sample at higher temperatures seems to be unnecessary as single phased $Gd_{0.90}Tb_{0.10}SrAl_3O_7$

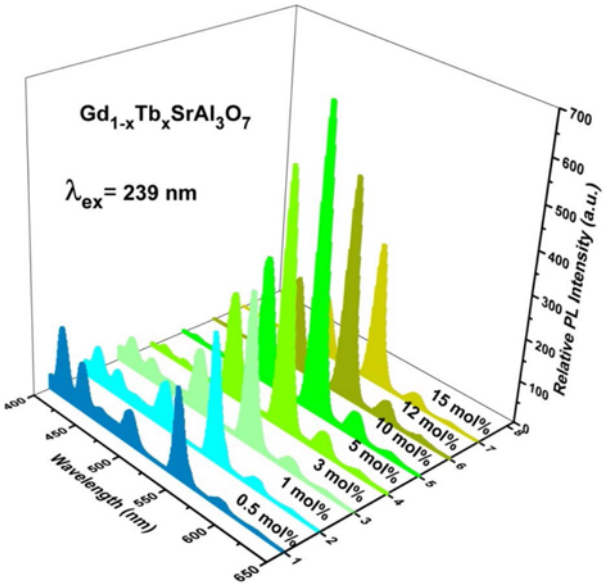

Fig. 5. Photoluminescence emission spectra of $Gd_{(1-x)}Tb_xSrAl_3O_7$ nanophosphors doped with different mol. % of terbium ions sintered at 550°C, λ_{ex} = 239 nm.

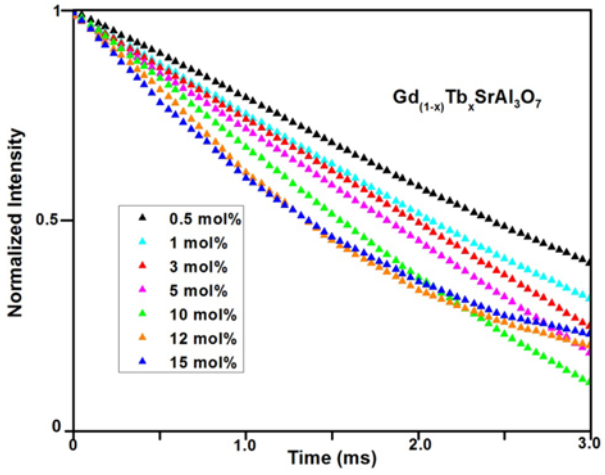

Fig. 6. Decay patterns of $Gd_{(1-x)}Tb_xSrAl_3O_7$ nanophosphors doped with different mol. % of terbium ions sintered at 550°C, λ_{ex} = 239 nm.

nanophosphors were obtained at low temperature (550°C) by SCS. The crystallization temperature, 550°C and duration (1 h) is low as compared to that of EDTA sol-gel process because all the precursors get homogeneously mixed at a molecular level that promote the crystallinity of $GdSrAl_3O_7$ at much lower temperature in SCS.

Figure 5 shows the PL spectra of all $Gd_{1-x}Tb_xSrAl_3O_7$ powders (0.5 to 15 mol. %) sintered at 550°C on exciting them at 239 nm wavelength. It is well known that visible luminescence of Tb^{3+} ions is mainly due to both $^5D_3 \rightarrow {}^7F_j$ and $^5D_4 \rightarrow {}^7F_j$ transitions. For terbium ions, blue emission at wavelength below 480 nm can be attributed to the $^5D_3 \rightarrow {}^7F_{5,4,3}$ transitions while transitions from $^5D_4$ to $^7F_{6,5,4,3}$ above 480 nm represent emission in green spectral region. Luminescence dynamics of $GdSrAl_3O_7$ greatly varies with terbium ions concentration as shown in Fig. 5. In $Gd_{1-x}Tb_xSrAl_3O_7$, all the characteristic emission peaks corresponding to $^5D_3 \rightarrow {}^7F_5$ (415 nm), $^5D_3 \rightarrow {}^7F_4$ (438 nm) and $^5D_3 \rightarrow {}^7F_5$ (458 nm) transitions in blue region and $^5D_4 \rightarrow {}^7F_6$ (492 nm), $^5D_4 \rightarrow {}^7F_5$ (544 nm), $^5D_3 \rightarrow {}^7F_4$ (588 nm) and $^5D_3 \rightarrow {}^7F_3$ (622 nm) transitions in green region were observed.[35] It is quite noticeable that at lower concentration, emissions from both of the excited state were observed. However, the luminescent intensity of $^5D_3 \rightarrow {}^7F_j$ transitions decreased with the increasing terbium contents in $GdSrAl_3O_7$ nanophosphors whereas that of the $^5D_4 \rightarrow {}^7F_5$ (544 nm) enhanced, reaching a maximum at 10 mol. %. As doping of terbium ions exceeds this optimum concentration (10 mol. %), the emission intensity of $^5D_4 \rightarrow {}^7F_5$ transition drops significantly. This concentration quenching may be attributed to non-radiative multiphonon cross relaxation by AlO_4^{5-} group in host which is not able to bridge the gaps between $^5D_3$ and $^5D_4$ energy states of terbium. As the Tb^{3+} ions contents increases above the optimum value, the distance between adjacent ions decreases in the host which facilitate the energy transfer between neighboring terbium ions.[15] Hence, most of the Tb^{3+} ions in $^5D_3$ relax nonradiatively to $^5D_4$ through multiphonon interactions with neighboring Tb^{3+} ions, which is described as:

$$Tb^{3+}(^5D_3) + Tb^{3+}(^7F_6) \rightarrow Tb^{3+}(^5D_4) + Tb^{3+}(^7F_0)$$

To better understand the quenching mechanism, the photoluminescence decay curves corresponding to $^5D_4 \rightarrow {}^7F_5$ transitions of Tb^{3+} ions in $GdSrAl_3O_7$ host lattice were characterized as shown in Fig. 6. These decay curves well fitted by single exponential behavior, represented by the equation;

$$I = I_0 \exp(-t/\tau) \quad (3)$$

where τ is the radiative decay time, I and I_0 are the luminescence intensities at time t and 0, respectively at low concentration (x < 10 mol. %) but deviated to non- exponential behavior when terbium doping exceeds the critical concentration (x > 10 mol. %).The average life time calculated for $Gd_{1-x}Tb_xSrAl_3O_7$ nanophosphors are 1.72 ms, 1.61 ms, 1.60 ms, 1.39 ms, 1.11 ms, 0.66 ms and 0.60 ms corresponding to 0.5, 1, 3, 5, 10, 12 and 15 mol. %, respectively. The Commission Internationale de L'Eclairage (CIE) chromaticity coordinates of $GdSrAl_3O_7$ doped with different Tb^{3+} contents, calculated from their corresponding emission spectra on excitation at 239 nm are summarized in Table 2. Compared with terbium doped green phosphor, Y_2O_3 (0.319, 0.597),[36] $Gd_{1-x}Tb_xSrAl_3O_7$ nanophosphor at optimum concentration (10 mol. %) exhibits excellent color in green region (0.266, 0.611), which is in accordance with European

Table 2. CIE of $Gd_{(1-x)}Tb_xSrAl_3O_7$ nanophosphor doped with different contents of terbium ions sintered at 550°C, λ_{ex} = 239 nm and λ_{em} = 544 nm.

$Gd_{1-x}Tb_xSrAl_3O_7$	CIE Coordinates	
	x	*y*
0.5 mol. %	0.2058	0.2793
1 mol. %	0.2241	0.3878
3 mol. %	0.2328	0.4357
5 mol. %	0.2631	0.5850
10 mol. %	0.2680	0.6119
12 mol. %	0.2692	0.6038
15 mol. %	0.2645	0.6006

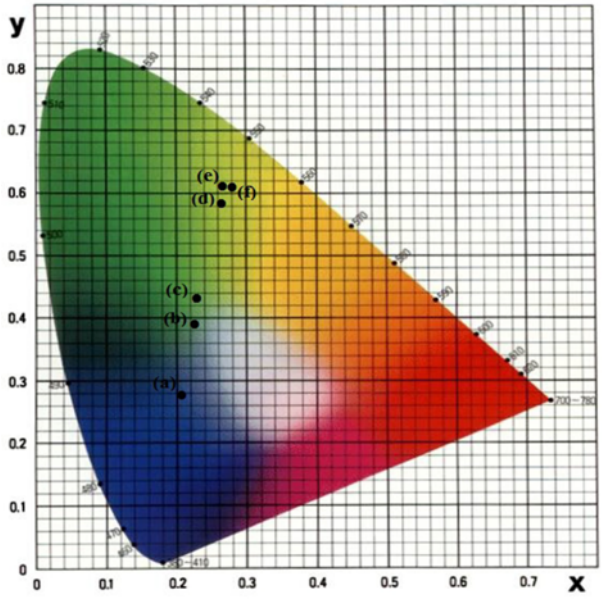

Fig. 7. CIE chromaticity diagram of $Gd_{(1-x)}Tb_xSrAl_3O_7$ nanophosphors for different terbium contents (a) 0.5 mol. %, (b) 1 mol. %, (c) 3 mol. % (d) 5 mol. % (e) 10 mol. % (f) 12 mol. % sintered at 550°C, λ_{ex} = 239 nm and λ_{em} = 544 nm.

Broadcasting Union standard colors (0.29, 0.60). Figure 7 clearly depicts that with the increasing concentration of dopant, the corresponding color tone shifts gradually from blue to green, confirming the CIE chromaticity coordinates are tunable by adjusting the concentration of Tb^{3+} ions in $GdSrAl_3O_7$ host.

4. CONCLUSIONS

In summary, single phased $GdSrAl_3O_7$ nanophosphors doped with Tb^{3+} ions were successfully synthesized by low cost and energy saving solution combustion process. In comparision with EDTA sol-gel method, SCS offers the benefit of short reaction time, low crystallization temperature and narrow size distribution of phosphor particles. Upon excitation at 239 nm, $Gd_{1-x}Tb_xSrAl_3O_7$ nanophosphors exhibit characteristic emission of terbium ions in blue and green spectral region. Their composition can be tuned from blue to green which lead to optimized luminescent properties. The decay curve imply that the optimum concentration is 10 mol. %. The excellent photoluminescence characteristics make it an attractive candidate for use in optical applications.

ACKNOWLEDGEMENT

One of the authors Ms. Sonika gratefully acknowledges the financial support in the form of Junior Research Fellowship (CSIR-UGC), New Delhi, India.

REFERENCES

1. J. W. Stouwdam and F. V. Veggel, *Nano Lett.* **2**, 733 (2002).
2. K. Kompe, H. Borchert, J. Storz, A. Lobo, S. Adam, T. Moller, and M. Haase, *Angew. Chem. Int. Ed.* **42**, 5513 (2003).
3. X. Wang, J. Zhuang, Q. Peng, and Y. D. Li, *Nature* **437**, 121 (2005).
4. R. Si, Y. W. Zhang, L. P. You, and C. H. Yan, *Angew. Chem. Int. Ed.* **44**, 3256 (2005).
5. T. Yu, J. Joo, Y. I. Park, and T. Hyeon, *J. Am. Chem. Soc*. **128**, 1786 (2006).
6. M. Ayvacikli, A. Ege, and N. Can, *Opt. Mater.* **34**, 138 (2011).
7. C. Feldmann, T. Justel, C. R. Ronda, and P. J. Schmidt, *Adv. Funct. Mater.* **13**, 511 (2003).
8. S.-A. Yan, J.-W. Wang, Y.-S. Chang, W.-S. Hwang, and Y.-H. Chang, *Opt. Mater.* **34**, 147 (2011).
9. X. Zhang and H. J. Seo, *J. Alloys Compd.* **509**, 2007 (2011).
10. Y. Shang, P. Yang, W. Wang, Y. Wang, N. Niu, S. Gai, and J. Lin, *J. Alloys Compd.* **509**, 837 (2011).
11. A. Bao, H. Yang, and C. Tao, *Curr. Appl. Phys.* **9**, 1252 (2009).
12. M. Malinowski, I. Pracka, P. Myziak, R. Piramidowicz, and W. Wolinski, *J. Lumin*. **72**, 224 (1997).
13. N. Kodama, Y. Tanii, and M. Yamaga, *J. Lumin*. **87**, 1076 (2000).
14. V. Singh, V. V. R. K. Kumar, R. P. S. Chakradhar, and H.-Y. Kwak, *Philosophical Magazine* **90**, 3095 (2010).
15. Sheetal, V. B. Taxak, Mandeep, and S. P. Khatkar, *J. Alloys Compd.* **549**, 135 (2013).
16. V. Singh, V. K. Rai, K. A. Shamery, J. Nordmann, and M. Hasse, *J. Lumin.* **131**, 2679 (2011).
17. V. Singh, S. Watanabe, T. K. Gundurao, and H.-Y. Kwak, *J. Fluoresc*. **21**, 313 (2011).
18. L. Zhou, W. C. H. Choy, J. Shi, M. Gong, and H. Liang, *J. Alloys Compds.* **463**, 302 (2008).
19. L. Zhou, W. C. H. Choy, J. Shi, M. Gong, H. Liang, and T. I. Yuk, *J. Solid State Chem.* **178**, 3004 (2005).

20. X. Zhang, J. Zhang, L. Liang, and Q. Su, *Mater. Res. Bull.* **40**, 281 (2005).
21. M. A. Kale, C. P. Joshi, S. V. Moharil, P. L. Muthal, and S. M. Dhopte, *J. Lumin.* **128**,1225 (2008).
22. B. Liu, D. Ding, Z. Liu, F. Chen, and C. Xia, *Solid State Lasers* **191**, 68 (2011).
23. W. R.-Romanowski, S. Golab, W. A. Pisarski, G. D.-Dzik, M. Berkowski, and A. Pajaczkowska, *Int. J. Electronics* **81**, 457 (1996).
24. W. R.-Romanowski, S. Golab, W. A. Pisarski, G. D.-Dzik, M. Berkowski, and A. Pajaczkowska, *J. Phys. Chem. Solids* **58**, 639 (1997).
25. M. Karbowiak, P. Gnutek, C. Rudowicz, and W. R. Romanowski, *Chem. Phys*. **387**, 69 (2011).
26. S.-I. Kubota. M. Izumi, H. Yamane, and M. Shimada, *J. Alloys Compds.* **283**, 95 (1999).
27. J. Yang, Y. Su, H. Li, X. Liu, and Z. Chen, *J. Alloys Compd.* **509**, 8008 (2011).
28. L.Wang, L. Shi, N. Liao, H. Jia, P. Du, Z. Xi, L. Wang, and D. Jin, *Mater. Chem. Phys.* **119**, 490 (2010).
29. B. Mari, K. C. Singh, M. Sahal, S. P. Khatkar, V. B. Taxak, and M. Kumar, *J. Lumin.* **131**, 587 (2011).
30. V. B. Taxak, Sheetal, Dayawati, and S. P. Khatkar, *Curr. Appl. Phys.* **13**, 594 (2013).
31. S. Ekambaram, M. Maaza, and K. C. Patil, *J. Alloys Compd.* **393**, 81 (2005).
32. S. T. Aruna and A. S. Mukasyan, *Curr. Opin. Solid State Mater. Sci*. **12**, 44 (2008).
33. G. M. Cai, F. Zheng, D. Q. Yi, Z. P. Jin, and X. L. Chen, *J. Lumin*. **130**, 910 (2010).
34. H. Wu, Y. Hu, F. Kang, L. Chen, X. Wang, G. Ju, and Z. Mu, *Mater. Resear. Bull*. **46**, 2489 (2011).
35. J. Liao, B. Qiu, H. Wen, and W. You, *Opt. Mater*. **31**, 1513 (2009).
36. J. Hao, S. A. Studenikin, and M. Cocivera, *J. Lumin.* **93**, 313 (2001).